Photoelectron imaging of the SO_3 anion: Vibrational resolution in photoelectron angular distributions.

Cate S. Anstöter and Jan R. R. Verlet

Department of Chemistry, Durham University, Durham DH1 3LE, United Kingdom

Abstract

The photoelectron imaging of the pyramidal sulphite radical monoanion is presented in the photon energy range spanning 3.10 to 4.45 eV. Two features are seen corresponding to formation of the ground electronic state of the neutral and to thermionic emission, which is seen for $h\upsilon$ > 3.7 eV. Photoelectron spectra corresponding to direct detachment show vibrational structure associated with the υ_2 umbrella mode of the neutral. A similar structure is seen in the photoelectron angular distributions. The photoelectron angular distributions were modelled and agree with experiment. However, we cannot provide an explanation for the observed vibrational structure in the photoelectron angular distributions. The observed thermionic emission is assigned to the excitation to a pair of degenerate Feshbach resonances, which can internally convert and subsequently emit electrons statistically.

1. Introduction

Anion photoelectron spectroscopy has been extensively used to probe the structure of closed- and open-shell anionic and neutral molecules.[1–3] The advent of charged-particle imaging,[4] which was transformed by the development of velocity-map imaging by Eppink and Parker,[5] provides velocity vector information. For photoelectrons, as all particles have the same mass, this information takes the form of photoelectron spectra with corresponding photoelectron angular distributions (PADs). The PADs can be described, for a single-photon transition with linear polarisation, by[6–8]

$$I(\theta) = \sigma / 4\pi \, [1 + \beta_2 P_2(\cos\theta)],$$

where I is the photoelectron signal at the angle θ between the polarisation vector of the light and the outgoing electron velocity vector; σ is the total detachment cross section; β_2 the anisotropy parameter; and $P_2(\cos\theta)$ the second-order Legendre polynomial. The PADs can thus be defined through a single parameter, β_2, which can take on values between the limiting values of +2 for a $I(\theta)$ α $\cos^2\theta$ distribution and −1 for a $I(\theta)$ α $\sin^2\theta$ distribution. The PADs contain important electronic structure information about the detachment process because the PADs are determined by the molecular orbital from which the electron is detached.[8] Hence, photoelectron imaging does not only provide direct structural information through the Franck-Condon factors between the anion initial and neutral final states, but it also provides electronic structure information. Generally, these two aspects have been considered separately. Specifically, the spectrally dispersed electrons in kinetic energy, eKE, reveal the vibrational levels in the final state, while the PADs are analysed to provide a symmetry for the overall transition.[9,10] Here, we present the photoelectron imaging of SO_3^- and show that β_2 dispersed in eKE also shows structure that can be directly correlated with the vibrational features seen in the photoelectron spectrum. Surprisingly, these appear to show greater sensitivity than the photoelectron spectrum.

Sulphite (SO_3) has attracted interest predominantly because of its roles in atmospheric chemistry.[11–22] In contrast, its anion has received significantly less attention.[23–27] Of immediate relevance to the current work is a previous photoelectron spectroscopic study by Dobrin *et al.*[28] The ground state of the anion is pyramidal while the neutral is planar, leading to a very broad photoelectron spectrum with the dominant vibrational progression being the umbrella mode that connects the ground states of the neutral and the anion. The 0-0 transition was not visible because of negligible Franck-Condon overlap. Dobrin *et al.* also showed that the PADs for emission from SO_3^- peaks were parallel to the polarisation vector of the light (i.e. $\beta_2 > 0$) by rotating the polarisation of the light field with respect to their detector. Here we build upon this work and present a photoelectron imaging study using a range of photon energies. The added dimension offered by the PADs provides insight into the electronic structure of SO_3^-. Sanov and coworkers have developed qualitative descriptions of the PADs based on the symmetry of the initial orbital.[29–31] This model provides an intuitive guide to the dominant character of the orbital. For example, it predicts that s-type or σ molecular orbitals generally have $\beta_2 > 0$, while π molecular orbitals generally have $\beta_2 < 0$. Dobrin *et al.* showed that the PADs for direct detachment from SO_3^- have $\beta_2 > 0$, which is qualitatively consistent with detachment from the totally symmetric $^2A_1$ ground state.[28] A more quantitative analysis can be offered by modelling the PADs based on the photodetachment from the relevant initial orbital. Krylov and coworkers used a Dyson orbital approach, where the Dyson orbital is the one-electron molecular orbital from which the electron is lost in the photodetachment, to compute laboratory-frame PADs as a function of eKE.[32–34] These have proven to be quite reliable for photodetachment and have been exploited by us and others to probe a range of anion detachment PADs,[35–42] including ones with conformational flexibility.[43,44] We use this method here to assess the measured PADs.

2. Methods

2.1 Experimental

The SO_3^- gas-phase synthesis presented here differs significantly from that used by Dobrin *et al.*. In their approach, a harsh electric discharge of a supersonic expansion of a mix containing Ar, N_2O and SO_2 was used.[28] While SO_3^- was clearly produced, they also noted the production of S_2O^-, which is isobaric. Moreover, discharge sources often produce vibrationally hot ions as the vibrations are inefficiently quenched in the ensuing supersonic expansion. In the present experiment, SO_3^- was produced through collision-induced dissociation of an electrosprayed precursor ion.[37,38] Specifically, 9,10-Anthraquinone-2,6-disulfonic acid disodium salt (Sigma Aldrich) was dissolved in methanol and electrosprayed in negative mode. Anions were transferred through a capillary into a vacuum chamber with several differentially pumped regions through which ions were drawn by RF ion guides. Between the first and second region, where the pressure differential is from 1 to 5×10^{-2} Torr, the ions were accelerated by 20 V through an orifice, which was sufficient to induce dissociation, with the dominant fragment being SO_3^-. The SO_3^- ion was then guided and thermalised through another set of ion guides that culminate in an ion trap at room temperature. The accumulated ions in the trap were subsequently injected at 10 Hz into a colinear Wiley-McLaren time-of-flight mass spectrometer.[45] At the focus of the mass-spectrometer, the SO_3^- ion packet was mass-selected by timing a nano-second laser pulse from a Nd:YAG-pumped OPO. The generated photoelectrons were velocity-map imaged using a two-electrode design with a resistive glass tube.[46] Photoelectrons were amplified using a dual multichannel plate detector and impacted onto a phosphor screen. The position sensitive events were captured using a CCD camera and accumulated over several 1000 laser shots. The raw photoelectron images were analysed using polar onion peeling[47] and calibrated using the photoelectron

spectrum of iodide. The overall spectral resolution was on the order of 5% of the eKE. Details of the instrument are provided elsewhere.[48]

2.2 Computational

The ground state geometries of the SO_3 anion and neutral were optimized at the coupled cluster singles and doubles (CCSD) with aug-cc-pVDZ level.[49,50] Geometries were confirmed to be energetic minima by diagonalization of the Hessian. Vertical excitation energies of the anion were calculated with EOM-EE-CCSD/aug-cc-pVDZ.[51] The Dyson orbital for the photodetachment of the SO_3 anion was obtained using the ionisation potential implementation of EOM-CCSD (EOM-IP-CCSD), using a restricted open Hartree Fock reference and the basis set above. The PADs for this direct detachment channel was modelled using ezDyson 4.0,[52] developed by Krylov and coworkers. All *ab initio* calculations were obtained using the QChem 5.0 computational package.[53]

The EOM-IP-CCSD calculation used to obtain the Dyson orbital can also provide a direct calculation for the vertical detachment energy, VDE. The VDE corresponds to the first EOM-IP state, which represents the difference in energy between the ground state of the anion (the EOM-IP reference state) and the ground state of the neutral (the target EOM-IP state).[32,33]

3. Results

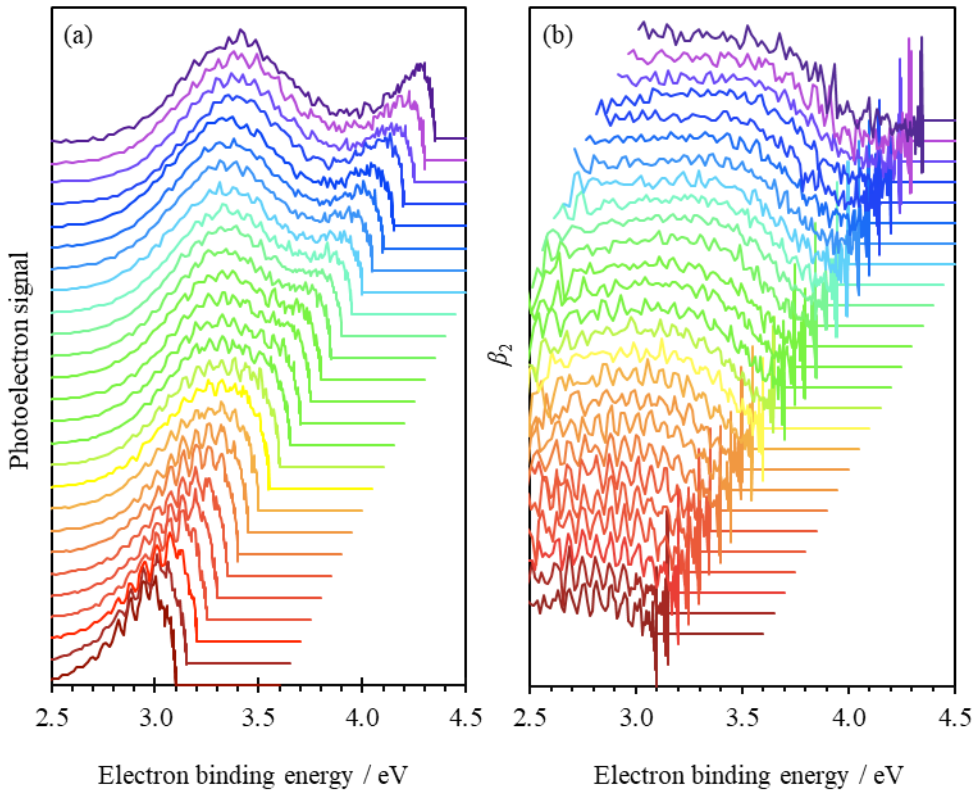

Figure 1: Photoelectron spectra taken in the range $3.10 \leq h\upsilon \leq 4.45$ eV with 0.05 eV increments (a) and corresponding β_2 spectra (b). Horizontal lines indicate the zero levels (in terms of signal and β_2). Successive spectra are offset by +0.4. The photoelectron spectra are normalised to a maximum intensity of 1. β_2 spectra are on their absolute scale.

The photoelectron spectra taken at photon energies in the range $3.10 \leq h\upsilon \leq 4.45$ eV with 0.05 eV increments are plotted in Figure 1(a) in terms of their electron binding energy, eBE = $h\upsilon$ − eKE. To emphasize spectral changes as a function of $h\upsilon$ and to aid comparison between spectra, each photoelectron spectrum has been normalised to a maximum intensity of 1 and have been offset relative to each other with the zero-signal level indicated by the respective horizontal lines.

The photoelectron spectra in Figure 1(a) are dominated by a single broad feature. Between $3.10 \leq h\upsilon \lesssim 3.40$ eV, the maximum of the photoelectron peak appears to shift to

higher eBE, while for $h\nu$ > 3.4 eV, the peak maximum remains constant at eBE ~ 3.4 eV. This peak corresponds to direct detachment from the ground state of the SO_3 anion to the ground state of the SO_3 neutral and the maximum in the photoelectron spectrum provides a measure of the vertical detachment energy, VDE, which we estimate to be at 3.4±0.1 eV. The vibrational structure seen in the direct detachment feature, particularly at lower $h\nu$, arises from the large structural displacement between the two ground state equilibrium geometries. The spacing between vibrational peaks determined from the photoelectron spectra is ~500 cm^{-1}. The apparent shift towards lower VDE at $h\nu$ < 3.4 eV arises because these photon energies are insufficient to access the maximum of the Franck-Condon envelope. This also observed in similar geometric differences between anion and neutral ground states, such as in the photoelectron spectra of $C_6F_6^-$.[54]

The PADs quantified by the parameter β_2 are shown in Figure 1(b) in the same eBE and $h\nu$ range as the photoelectron spectra. Parts of these β_2 spectra are omitted as the photoelectron intensity in these ranges is too low to make a physically meaningful assignment of the PADs. As with the photoelectron spectra, the β_2 spectra are offset from each other to aid comparison. The β_2 = 0 level is indicated by the respective horizontal lines and each successive spectrum is offset by β_2 = +0.4. The primary purpose of Figure 1(b) is to show the qualitative trends as a function of $h\nu$ and a more quantitative consideration is offered below. Figure 1(b) shows that β_2 across the direct detachment feature is positive, indicating that the photoelectrons are predominantly ejected parallel to the polarisation axis. Surprisingly, the β_2 spectra also appear to show oscillations that appear to reflect the vibrational structure seen in the photoelectron spectra.

The correspondence between vibrational peaks in the photoelectron spectra and β_2 spectra is shown more clearly in Figure 2, for a representative spectrum at $h\nu$ = 3.25 eV. The correlation between the structure in the photoelectron spectra and β_2 spectra is highlighted by the dashed vertical lines. Rather unexpectedly, the β_2 value shows crisp

vibrational structure and appears to be more resolved towards lower eBE (higher kinetic energy) than the photoelectron spectrum. The additional and more resolved features offer an opportunity to determine the spacing between peaks more accurately. Figure 3 shows the β_2 spectrum (as a function of eKE) at $h\upsilon$ = 3.25 eV, superimposed by a fit to this date of a sinusoidal function which has an increasing offset with increasing eKE. Peaks up to eKE ~ 0.7 eV are very well reproduced by the fit function. Beyond this eKE, the photoelectron signal is too low to determine a meaningful β_2 value and these data are dominated by noise. The frequency of the sinusoidal oscillation yields a vibrational spacing of 517±10 cm^{-1}, which is essentially constant the 11 vibrational levels seen.

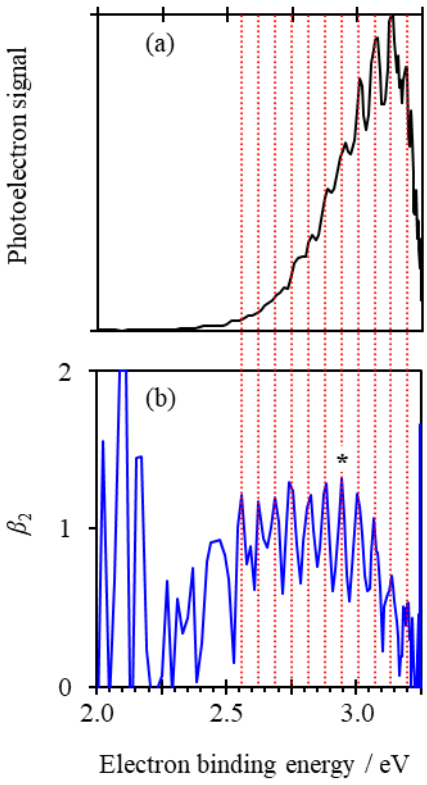

Figure 2: Photoelectron spectrum taken at $h\upsilon$ = 3.25 eV (a) and corresponding β_2 spectrum (b). Vertical dashed lines are guides to the eye to show the correlation between oscillations in the β_2 spectrum with the peaks in the photoelectron spectrum.

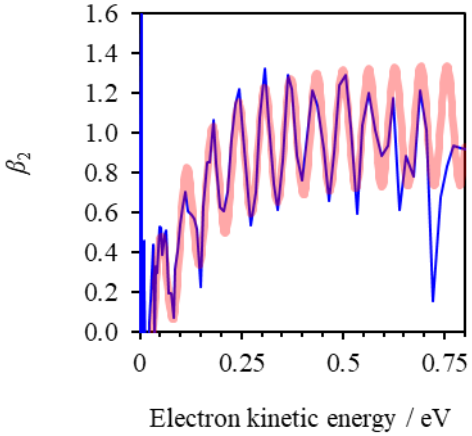

Figure 3: β_2 spectrum following detachment at $h\upsilon$ = 3.25 eV (blue), with superimposed a fit based on a constant amplitude sine wave with an increasing offset (transparent red).

In addition to the direct detachment feature, a second photoelectron feature can be seen at higher excitation energies in Figure 1(a). This feature appears as a peak in the photoelectron spectra that shifts in eBE with increasing $h\upsilon$. In the PADs, this feature is broadly isotropic ($\beta_2 \sim 0$).

To supplement the experiments, we have also performed *ab initio* calculations. The SO_3 anion has a C_{3v} pyramidal minimum energy structure, whereas the SO_3 neutral has a planar D_{3h} minimum energy structure, in agreement with previous computational work.[55,56] The long vibrational progression arising from the υ_2 umbrella mode of the neutral corresponds to the pyrimidalisation of the planar geometry. The EOM-IP-CCSD calculation used to obtain the Dyson orbital predicts VDE = 3.51 eV. This computed VDE is in good agreement with the experimental VDE = 3.4±0.1 eV determined here. The very broad vibrational progression renders the experimental determination of the adiabatic detachment (ADE or electron affinity) difficult because it probably has a very small (negligible) Franck-Condon factor and, hence, we refrain from assigning it. The literature value ADE = 1.9±0.1 eV.[26]

Figure 4 shows the Dyson orbital for SO_3^- detachment together with the computed β_2 as a function of eKE. Also included are experimentally determined β_2 values. Because of the observed oscillations in the β_2 spectra, we have determined the β_2 value for a given eKE by taking the β_2 value at the peak of a specific vibration and tracking its value for different $h\upsilon$ (*i.e.* the vibrational mode stays at a specific eBE but shifts with eKE as $h\upsilon$ is varied). We have chosen the vibrational mode at eBE = 2.95 eV (see asterisk in Figure 2(b)). Choosing different modes does not change the results significantly. The result of the analysis is shown in Figure 4 and β_2 values have a typical error of ±0.1. Overall, excellent qualitative agreement is seen between the experimental and computed β_2 values. The theoretical curve shows that, at low eKE, β_2 is more isotropic, and with increasing eKE, this tends to a value β_2 = +1.7. The experimental data shows the same trend but, on the whole, it has a slightly lower value of β_2 = +1.5.

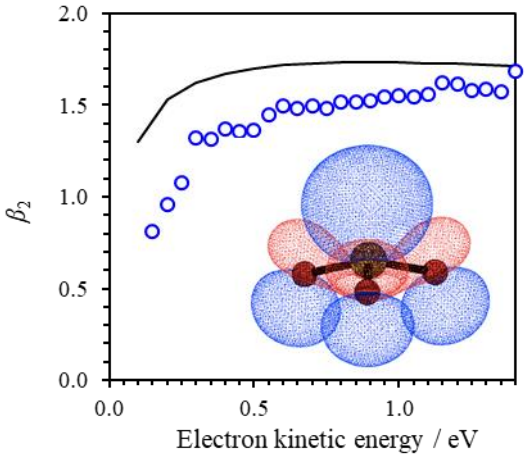

Figure 4: Calculated (solid line) and measured (symbols) β_2 parameters. The measured values are determined for a specific vibrational mode in the photoelectron spectra taken at several different $h\upsilon$. The Dyson orbital used to compute the β_2 spectrum is shown.

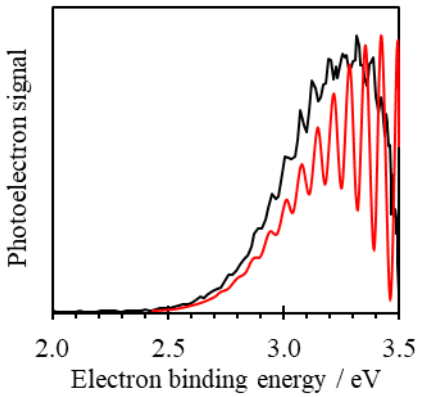

Figure 5: Measured (black line) and simulated (red line) photoelectron spectrum of SO_3^- taken at 3.5 eV. The simulation was adopted from reference 28.

4. Discussion

The spectroscopic parameters determined in the present work are in good agreement with previous works.[25–28,57] Dobrin *et al.* performed an in-depth analysis of their photoelectron spectrum taken at 355 nm. They found that VDE = 3.41±0.01 eV and performed a detailed Franck-Condon analysis of the vibrational progression. Their photoelectron spectrum yielded a vibrational frequency of υ_2 = 548±80 cm^{-1} for the SO_3 neutral, which is expected to be highly excited given the difference in geometries between anion and neutral ground states. High-resolution gas-phase IR spectroscopy has determined υ_2 = 498 cm^{-1}.[19,58] In the present experiment, we have determined υ_2 = 517±10 cm^{-1} from Figure 3. This is in good agreement with the value from Dobrin *et al.* but slightly higher than that determined from the IR spectrum. The higher value quoted by Dobrin *et al.* compared to that from the IR spectrum was rationalised by the high vibrational quanta of υ_2 accessed in the neutral (υ = 22 at the Franck-Condon peak based on a Franck-Condon simulation) and a possible negative quadratic or cubic anharmonicity constant.[28] As the υ_2 determined here is close to that determined for the (υ = 1 ← υ = 0) transition,[19,58] but slightly higher and outside our uncertainty range, there does appear to be a slight

negative anharmonicity, similar to that seen in the methyl radical.[59] Nevertheless, the anharmonicity is very small. Figure 5 shows the computed photoelectron spectrum based on the Franck-Condon simulation presented by Dobrin *et al.*[28] Ignoring the fact the difference between computed and measured vibrational frequency, the agreement with the photoelectron spectrum measured here is excellent. In fact, it is better than the agreement with the photoelectron spectrum by Dobrin *et al.*, which showed signal extending to eBE < 2.0 eV.[28] We suspect that the discrepancy may be due to a high internal energy of SO_3^- in the experiments by Dobrin *et al.*: SO_3^- formed in a discharge source can lead to high and non-thermal vibrational internal excitation. Note also that the discrepancy at highest eBE (low eKE) is due to threshold behaviour which is not accounted for in the simulation.

The PADs offer added insight into the *electronic* structure of the anion. Based on the good agreement between experimental and computed β_2 in Figure 4, we can be confident that the Dyson orbital shown represents the highest occupied molecular orbital (HOMO) of SO_3^- and the ground state is $X\ ^2A_1$. This is in agreement with the conclusion form Dobrin *et al.*.[28]

Based on the measured and computed PADs, we conclude that the outgoing wave is predominantly of p-character. Hence, a centrifugal barrier is present for the emission leading to the Wigner threshold behaviour where the detachment cross section scales as $eKE^{3/2}$.[60] The consequence of this is that the cross section for detachment at the highest eBE for a given spectrum (corresponding to lowest eKE) rises initially as shown most clearly in Figure 2(a). The associated β_2 at low eKE becomes more isotropic as the weighting of any s-partial waves increases. This is clearly shown in Figure 2(b) and 3 and accounts for the increasing offset required in the fit-function.

The most striking aspect of the current work is the apparent vibrational structure in the β_2 spectra. Vibrational structure in the photoelectron spectra comes about from the excitation of vibrational states in the neutral upon photodetachment (*i.e.* a simple Franck-Condon argument). In the case of infinite resolution and ignoring temperature and rotation, this should produce a "stick" spectrum. Each of these "sticks" will have an associated PAD, which, according to the above arguments, will be predominantly of p-character. In between, as there is no signal, there can be no defined β_2 value. In the present experiment, the vibrational peaks are broadened/congested by Boltzmann factors and the finite (and not very good) resolution of our experiment. This means that each vibrational peak has overlap with the neighbouring peak (Figure 2(a)). However, the β_2 value for each of these peaks should remain what they were in the infinite resolution case and no oscillations are expected. Gradual variation for different vibrational levels may be expected (as seen in O_2^- photodetachment),[61] but given the resolution in the current experiment, one might expect these to appear then as small and shallow steps in the β_2 spectrum rather than the dramatic oscillations that are observed in Figure 2(b) and 3. Perhaps the most obvious consideration is that there is a constant signal (isotropic) background in the image that would force $\beta_2 \rightarrow 0$ when the photoelectron signal is small. This could arise from a second detachment channel. For example, if an excited state ~2.6 eV above the anion ground state was present, it could lead to autodetachment providing a signal with different anisotropy. Our calculations show that a degenerate pair of resonances can be excited, but these are located at 3.51 eV and are discussed further below. There is an additional excited state at 2.54 eV (SOMO → LUMO), but it is optically forbidden with an oscillator strength of 0 and its contribution to the photoelectron signal would be very small. Remarkably, even when vibrational structure cannot be resolved in the photoelectron spectrum, we appear to be able to resolve the oscillations in the β_2 spectrum (see Figure 2(b)). PADs are determined by the interference between partial

waves of the outgoing photoelectron. One might therefore invoke an interference mechanism to explain the oscillations. However, the electronic states are not changing with eKE and vibrational quantum levels do not have a relative symmetry, so this does not explain the observations either. Finally, one could suspect that the analysis method of the raw image could introduce artefacts. Here, we used polar onion peeling, but other analysis methods were also used and these show similar oscillations in the β_2 spectrum. In the end, we simply do not have a clear explanation for the observation.

Finally, we briefly comment on the second emission channel observed $h\nu > 3.7$ eV. With increasing $h\nu$, this feature appears to have an increasing eBE. That is to say, the eKE of this peak is essentially constant and peaks at eKE ~ 0.07 eV. Furthermore, the β_2 associated with this feature is close to zero – *i.e.* the emission is isotropic.[62] Features that appears near zero eKE are often signatures of thermionic emission from the anion ground state.[63–70] Specifically, photoexcitation from the ground state can access excited states of the anion that lie in the continuum (resonances). These resonances can then decay either by autodetachment that may include some exchange of energy (electronic to nuclear) so that the electron leaves with less kinetic energy, or nuclear dynamics on the resonance may outcompete autodetachment and internal conversion can reform the ground electronic state of the anion.[69,71–73] In the latter case, the total energy in the ground state anion remains above that of the neutral. Electron emission becomes a statistical process reliant on internal vibrational energy redistribution. Because of the statistical nature, the emission is generally peaked at low eKE with an exponentially decaying spectral distribution. Moreover, as the timescale for the emission can be many microseconds, many rotational dephasing precedes electron emission so that the PAD is expected to be anisotropic ($\beta_2 = 0$). As Feshbach resonances, the autodetachment lifetime is expected to be relatively long (typically on the order of several 100s of femtoseconds), so that internal conversion could compete. Hence, we suspect that the emission at low eKE is indeed

thermionic emission from the reformed ground state anion. This is supported by the measured $\beta_2 = 0$ for this feature. Additionally, the shape of the emission spectrum is consistent with thermionic emission. For species with relatively high symmetry, the cross-section rises first before decaying exponentially.[66] In the present case, electron emission will occur at the C_{3v} geometry to enable emission at the adiabatic binding energy. This relatively high symmetry will lead to the observed signal rise, similar to the case of C_{60}^- thermionic emission.[66]

Acknowledgement

We thank Chris Sparling and Dave Townsend (Heriot-Watt University) for analysing photoelectron images using different methodologies and for insightful discussions. We are grateful to the European Research Council (306536) for funding.

References

(1) Turner, D. W. Molecular Photoelectron Spectroscopy. *Philos. Trans. R. Soc. Math. Phys. Eng. Sci.* **1970**, *268* (1184), 7–31. https://doi.org/10.1098/rsta.1970.0059.

(2) Wenthold, P. G.; Lineberger, W. C. Negative Ion Photoelectron Spectroscopy Studies of Organic Reactive Intermediates. *Acc. Chem. Res.* **1999**, *32* (7), 597–604. https://doi.org/10.1021/ar960121x.

(3) Ervin, K. M.; Lineberger, W. C. Photoelectron Spectroscopy of Molecular Anions. In *Advances in Gas Phase Ion Chemistry*; Adams, N. G., Babcock, L. M., Eds.; JAI Press: Greenwich, 1992; p 121.

(4) Chandler, D. W.; Houston, P. L. Two-Dimensional Imaging of State-Selected Photodissociation Products Detected by Multiphoton Ionization. *J. Chem. Phys.* **1987**, *87* (2), 1445. https://doi.org/10.1063/1.453276.

(5) Eppink, A. T. J. B.; Parker, D. H. Velocity Map Imaging of Ions and Electrons Using Electrostatic Lenses: Application in Photoelectron and Photofragment Ion Imaging of Molecular Oxygen. *Rev. Sci. Instrum.* **1997**, *68* (9), 3477–3484. https://doi.org/10.1063/1.1148310.

(6) Cooper, J.; Zare, R. N. Angular Distribution of Photoelectrons. *J. Chem. Phys.* **1968**, *48* (2), 942–943. https://doi.org/10.1063/1.1668742.

(7) Cooper, J.; Zare, R. N. Erratum: Angular Distribution of Photoelectrons. *J. Chem. Phys.* **1968**, *49* (9), 4252–4252. https://doi.org/10.1063/1.1670761.

(8) Reid, K. L. Photoelectron Angular Distributions. *Annu. Rev. Phys. Chem.* **2003**, *54* (1), 397–424. https://doi.org/10.1146/annurev.physchem.54.011002.103814.

(9) Sanov, A.; Mabbs, R. Photoelectron Imaging of Negative Ions. *Int. Rev. Phys. Chem.* **2008**, *27* (1), 53–85. https://doi.org/10.1080/01442350701786512.

(10) Mabbs, R.; Grumbling, E. R.; Pichugin, K.; Sanov, A. Photoelectron Imaging: An Experimental Window into Electronic Structure. *Chem. Soc. Rev.* **2009**, *38* (8), 2169–2177. https://doi.org/10.1039/b815748k.

(11) Wayne, R. P. Chemistry of Atmospheres - An Introduction to the Chemistry of the Atmospheres of Earth, the Planets, and Their Satellites (2nd Revised and Enlarged Edition). *Oxf. Engl. N. Y. Oxf. Univ. Press 1991 460 P* **1991**.

(12) Kolb, C. E.; Jayne, J. T.; Worsnop, D. R.; Molina, M. J.; Meads, R. F.; Viggiano, A. A. Gas Phase Reaction of Sulfur Trioxide with Water Vapor. *J. Am. Chem. Soc.* **1994**, *116* (22), 10314–10315. https://doi.org/10.1021/ja00101a067.

(13) Jayne, J. T.; Pöschl, U.; Chen, Y.; Dai, D.; Molina, L. T.; Worsnop, D. R.; Kolb, C. E.; Molina, M. J. Pressure and Temperature Dependence of the Gas-Phase Reaction of SO3 with H2O and the Heterogeneous Reaction of SO3 with H2O/H2SO4 Surfaces. *J. Phys. Chem. A* **1997**, *101* (51), 10000–10011. https://doi.org/10.1021/jp972549z.

(14) Lovejoy, E. R.; Hanson, D. R.; Huey, L. G. Kinetics and Products of the Gas-Phase Reaction of SO3 with Water. *J. Phys. Chem.* **1996**, *100* (51), 19911–19916. https://doi.org/10.1021/jp962414d.

(15) Pommerening, C. A.; Bachrach, S. M.; Sunderlin, L. S. Addition of Protonated Water to SO3. *J. Phys. Chem. A* **1999**, *103* (9), 1214–1220. https://doi.org/10.1021/jp984104w.

(16) Meijer, E. J.; Sprik, M. A Density Functional Study of the Addition of Water to SO3 in the Gas Phase and in Aqueous Solution. *J. Phys. Chem. A* **1998**, *102* (17), 2893–2898. https://doi.org/10.1021/jp972146z.

(17) Morokuma, K.; Muguruma, C. Ab Initio Molecular Orbital Study of the Mechanism of the Gas Phase Reaction SO3 + H2O: Importance of the Second Water Molecule. *J. Am. Chem. Soc.* **1994**, *116* (22), 10316–10317. https://doi.org/10.1021/ja00101a068.

(18) Hofmann, M.; Schleyer, P. v. R. Acid Rain: Ab Initio Investigation of the H2O.Cntdot.SO3 Complex and Its Conversion to H2SO4. *J. Am. Chem. Soc.* **1994**, *116* (11), 4947–4952. https://doi.org/10.1021/ja00090a045.

(19) Ortigoso, J.; Escribano, R.; Maki, A. G. The N2 and N4 IR Bands of SO3. *J. Mol. Spectrosc.* **1989**, *138* (2), 602–613. https://doi.org/10.1016/0022-2852(89)90021-0.

(20) Lloyd, D. R.; Roberts, P. J.; Hillier, I. H.; Shenton, I. C. On the Photoelectron Spectrum of Sulphur Trioxide. *Mol. Phys.* **1976**, *31* (5), 1549–1556. https://doi.org/10.1080/00268977600101221.

(21) Henfrey, N. F.; Thrush, B. A. The N3 Band of SO3 at High Resolution. *Chem. Phys. Lett.* **1983**, *102* (2), 135–138. https://doi.org/10.1016/0009-2614(83)87379-5.

(22) Bork, N.; Kurtén, T.; Vehkamäki, H. Exploring the Atmospheric Chemistry of O $_2$ SO $_3$ − and Assessing the Maximum Turnover Number of Ion-Catalysed H $_2$ SO $_4$ Formation. *Atmospheric Chem. Phys.* **2013**, *13* (7), 3695–3703. https://doi.org/10.5194/acp-13-3695-2013.

(23) Hayon, E.; Treinin, A.; Wilf, J. Electronic Spectra, Photochemistry, and Autoxidation Mechanism of the Sulfite-Bisulfite-Pyrosulfite Systems. SO2-, SO3-, SO4-, and SO5- Radicals. *J. Am. Chem. Soc.* **1972**, *94* (1), 47–57. https://doi.org/10.1021/ja00756a009.

(24) Stanbury, D. M.; Holme, T. A.; Kafafi, Z. H.; Margrave, J. L. AB Initio Calculations and Matrix Ftir Studies of the Sulfur Trioxide Radical Anion. *Chem. Phys. Lett.* **1986**, *129* (2), 181–185. https://doi.org/10.1016/0009-2614(86)80193-2.

(25) Rothe, E. W.; Tang, S. Y.; Reck, G. P. Measurement of Electron Affinities of O3, SO2, and SO3 by Collisional Ionization. *J. Chem. Phys.* **1975**, *62* (9), 3829–3831. https://doi.org/10.1063/1.430941.

(26) Miller, T. M.; Viggiano, A. A.; Arnold, S. T.; Jayne, J. T. Thermal Electron Attachment to SO3. *J. Chem. Phys.* **1995**, *102* (15), 6021–6023. https://doi.org/10.1063/1.469336.

(27) Ding, C.-F.; Wang, X.-B.; Wang, L.-S. Photodetachment Photoelectron Spectroscopy of Doubly Charged Anions: S2O82−. *J. Chem. Phys.* **1999**, *110* (8), 3635–3638. https://doi.org/10.1063/1.478251.

(28) Dobrin, S.; Boo, B. H.; Alconcel, L. S.; Continetti, R. E. Photoelectron Spectroscopy of SO\textlesssub\textgreater3\textless/Sub\textgreater\textlesssup\textgreater-\textless/Sup\textgreater at 355 and 266 Nm. *J. Phys. Chem. A* **2000**, *104* (46), 10695–10700. https://doi.org/10.1021/jp0025680.

(29) Sanov, A. Laboratory-Frame Photoelectron Angular Distributions in Anion Photodetachment: Insight into Electronic Structure and Intermolecular Interactions. *Annu. Rev. Phys. Chem.* **2014**, *65* (1), 341–363. https://doi.org/10.1146/annurev-physchem-040513-103656.

(30) Khuseynov, D.; Blackstone, C. C.; Culberson, L. M.; Sanov, A. Photoelectron Angular Distributions for States of Any Mixed Character: An Experiment-Friendly Model for Atomic, Molecular, and Cluster Anions. *J. Chem. Phys.* **2014**, *141* (12), 124312. https://doi.org/10.1063/1.4896241.

(31) Grumbling, E. R.; Sanov, A. Photoelectron Angular Distributions in Negative-Ion Photodetachment from Mixed Sp States. *J. Chem. Phys.* **2011**, *135* (16), 164302. https://doi.org/10.1063/1.3653234.

(32) Oana, C. M.; Krylov, A. I. Dyson Orbitals for Ionization from the Ground and Electronically Excited States within Equation-of-Motion Coupled-Cluster Formalism: Theory, Implementation, and Examples. *J. Chem. Phys.* **2007**, *127* (23), 234106. https://doi.org/10.1063/1.2805393.

(33) Oana, C. M.; Krylov, A. I. Cross Sections and Photoelectron Angular Distributions in Photodetachment from Negative Ions Using Equation-of-Motion Coupled-Cluster Dyson Orbitals. *J. Chem. Phys.* **2009**, *131* (12), 124114. https://doi.org/10.1063/1.3231143.

(34) Gozem, S.; Gunina, A. O.; Ichino, T.; Osborn, D. L.; Stanton, J. F.; Krylov, A. I. Photoelectron Wave Function in Photoionization: Plane Wave or Coulomb Wave? *J. Phys. Chem. Lett.* **2015**, *6* (22), 4532–4540. https://doi.org/10.1021/acs.jpclett.5b01891.

(35) West, C. W.; Bull, J. N.; Hudson, A. S.; Cobb, S. L.; Verlet, J. R. R. Excited State Dynamics of the Isolated Green Fluorescent Protein Chromophore Anion Following

UV Excitation. *J. Phys. Chem. B* **2015**, *119* (10), 3982–3987. https://doi.org/10.1021/acs.jpcb.5b01432.

(36) Jagau, T.-C.; Dao, D. B.; Holtgrewe, N. S.; Krylov, A. I.; Mabbs, R. Same but Different: Dipole-Stabilized Shape Resonances in CuF – and AgF –. *J. Phys. Chem. Lett.* **2015**, *6* (14), 2786–2793. https://doi.org/10.1021/acs.jpclett.5b01174.

(37) Stanley, L. H.; Anstöter, C. S.; Verlet, J. R. R. Resonances of the Anthracenyl Anion Probed by Frequency-Resolved Photoelectron Imaging of Collision-Induced Dissociated Anthracene Carboxylic Acid. *Chem. Sci.* **2017**, *8* (4), 3054–3061. https://doi.org/10.1039/c6sc05405f.

(38) Anstöter, C. S.; Dean, C. R.; Verlet, J. R. R. Chromophores of Chromophores: A Bottom-up Hückel Picture of the Excited States of Photoactive Proteins. *Phys. Chem. Chem. Phys.* **2017**, *19* (44), 29772–29779. https://doi.org/10.1039/C7CP05766K.

(39) Woodhouse, J. L.; Henley, A.; Parkes, M. A.; Fielding, H. H. Photoelectron Imaging and Quantum Chemistry Study of Phenolate, Difluorophenolate, and Dimethoxyphenolate Anions. *J. Phys. Chem. A* **2019**, *123* (13), 2709–2718. https://doi.org/10.1021/acs.jpca.8b11121.

(40) Anstöter, C. S.; Gartmann, T. E.; Stanley, L. H.; Bochenkova, A. V.; Verlet, J. R. R. Electronic Structure of the Para-Dinitrobenzene Radical Anion: A Combined 2D Photoelectron Imaging and Computational Study. *Phys. Chem. Chem. Phys.* **2018**, *20*, 24019–24026. https://doi.org/10.1039/c8cp04877k.

(41) Weichman, M. L.; Kim, J. B.; Neumark, D. M. Slow Photoelectron Velocity-Map Imaging Spectroscopy of the *Ortho* -Hydroxyphenoxide Anion. *J. Phys. Chem. A* **2015**, *119* (23), 6140–6147. https://doi.org/10.1021/acs.jpca.5b00768.

(42) Laws, B. A.; Cavanagh, S. J.; Lewis, B. R.; Gibson, S. T. Wigner Near-Threshold Effects in the Photoelectron Angular Distribution of NO2–. *J. Phys. Chem. A* **2019**, *123* (48), 10418–10425. https://doi.org/10.1021/acs.jpca.9b09073.

(43) Anstöter, C. S.; Dean, C. R.; Verlet, J. R. R. Sensitivity of Photoelectron Angular Distributions to Molecular Conformations of Anions. *J. Phys. Chem. Lett.* **2017**, *8* (10), 2268–2273. https://doi.org/10.1021/acs.jpclett.7b00726.

(44) Anstöter, C. S.; Curchod, B. F. E.; Verlet, J. R. R. Geometric and Electronic Structure Probed along the Isomerisation Coordinate of a Photoactive Yellow Protein Chromophore. *Nat. Commun.* **2020**, *11* (1), 2827. https://doi.org/10.1038/s41467-020-16667-x.

(45) Wiley, W. C.; McLaren, I. H. Time-of-Flight Mass Spectrometer with Improved Resolution. *Rev. Sci. Instrum.* **1955**, *26* (12), 1150–1157. https://doi.org/10.1063/1.1715212.

(46) Horke, D. A.; Roberts, G. M.; Lecointre, J.; Verlet, J. R. R. Velocity-Map Imaging at Low Extraction Fields. *Rev. Sci. Instrum.* **2012**, *83* (6), 063101. https://doi.org/10.1063/1.4724311.

(47) Roberts, G. M.; Nixon, J. L.; Lecointre, J.; Wrede, E.; Verlet, J. R. R. Toward Real-Time Charged-Particle Image Reconstruction Using Polar Onion-Peeling. *Rev. Sci. Instrum.* **2009**, *80* (5), 053104. https://doi.org/10.1063/1.3126527.

(48) Lecointre, J.; Roberts, G. M.; Horke, D. A.; Verlet, J. R. R. Ultrafast Relaxation Dynamics Observed through Time-Resolved Photoelectron Angular Distributions. *J. Phys. Chem. A* **2010**, *114* (42), 11216–24. https://doi.org/10.1021/jp1028855.

(49) Purvis, G. D.; Bartlett, R. J. A Full Coupled-cluster Singles and Doubles Model: The Inclusion of Disconnected Triples. *J. Chem. Phys.* **1982**, *76* (4), 1910–1918. https://doi.org/10.1063/1.443164.

(50) Dunning, T. H. Gaussian Basis Sets for Use in Correlated Molecular Calculations. I. The Atoms Boron through Neon and Hydrogen. *J. Chem. Phys.* **1989**, *90* (2), 1007–1023. https://doi.org/10.1063/1.456153.

(51) Sekino, H.; Bartlett, R. J. A Linear Response, Coupled-Cluster Theory for Excitation Energy. *Int. J. Quantum Chem.* **1984**, *26* (S18), 255–265. https://doi.org/10.1002/qua.560260826.

(52) Gozem, S.; Krylov, A. I. *EzDyson V4*; http://iopenshell.usc.edu/downloads/ezdyson; http://iopenshell.usc.edu/downloads/ezdyson.

(53) Shao, Y.; Gan, Z.; Epifanovsky, E.; Gilbert, A. T. B.; Wormit, M.; Kussmann, J.; Lange, A. W.; Behn, A.; Deng, J.; Feng, X.; Ghosh, D.; Goldey, M.; Horn, P. R.; Jacobson, L. D.; Kaliman, I.; Khaliullin, R. Z.; Kuś, T.; Landau, A.; Liu, J.; Proynov, E. I.; Rhee, Y. M.; Richard, R. M.; Rohrdanz, M. A.; Steele, R. P.; Sundstrom, E. J.; Woodcock, H. L.; Zimmerman, P. M.; Zuev, D.; Albrecht, B.; Alguire, E.; Austin, B.; Beran, G. J. O.; Bernard, Y. A.; Berquist, E.; Brandhorst, K.; Bravaya, K. B.; Brown, S. T.; Casanova, D.; Chang, C.-M.; Chen, Y.; Chien, S. H.; Closser, K. D.; Crittenden, D. L.; Diedenhofen, M.; DiStasio, R. A.; Do, H.; Dutoi, A. D.; Edgar, R. G.; Fatehi, S.; Fusti-Molnar, L.; Ghysels, A.; Golubeva-Zadorozhnaya, A.; Gomes, J.; Hanson-Heine, M. W. D.; Harbach, P. H. P.; Hauser, A. W.; Hohenstein, E. G.; Holden, Z. C.; Jagau, T.-C.; Ji, H.; Kaduk, B.; Khistyaev, K.; Kim, J.; Kim, J.; King, R. A.; Klunzinger, P.; Kosenkov, D.; Kowalczyk, T.; Krauter, C. M.; Lao, K. U.; Laurent, A. D.; Lawler, K. V.; Levchenko, S. V.; Lin, C. Y.; Liu, F.; Livshits, E.; Lochan, R. C.; Luenser, A.; Manohar, P.; Manzer, S. F.; Mao, S.-P.; Mardirossian, N.; Marenich, A. V.; Maurer, S. A.; Mayhall, N. J.; Neuscamman, E.; Oana, C. M.; Olivares-Amaya, R.; O'Neill, D. P.; Parkhill, J. A.; Perrine, T. M.; Peverati, R.; Prociuk, A.; Rehn, D. R.; Rosta, E.; Russ, N. J.; Sharada, S. M.; Sharma, S.; Small, D. W.; Sodt, A.; Stein, T.; Stück, D.; Su, Y.-

C.; Thom, A. J. W.; Tsuchimochi, T.; Vanovschi, V.; Vogt, L.; Vydrov, O.; Wang, T.; Watson, M. A.; Wenzel, J.; White, A.; Williams, C. F.; Yang, J.; Yeganeh, S.; Yost, S. R.; You, Z.-Q.; Zhang, I. Y.; Zhang, X.; Zhao, Y.; Brooks, B. R.; Chan, G. K. L.; Chipman, D. M.; Cramer, C. J.; Goddard, W. A.; Gordon, M. S.; Hehre, W. J.; Klamt, A.; Schaefer, H. F.; Schmidt, M. W.; Sherrill, C. D.; Truhlar, D. G.; Warshel, A.; Xu, X.; Aspuru-Guzik, A.; Baer, R.; Bell, A. T.; Besley, N. A.; Chai, J.-D.; Dreuw, A.; Dunietz, B. D.; Furlani, T. R.; Gwaltney, S. R.; Hsu, C.-P.; Jung, Y.; Kong, J.; Lambrecht, D. S.; Liang, W.; Ochsenfeld, C.; Rassolov, V. A.; Slipchenko, L. V.; Subotnik, J. E.; Van Voorhis, T.; Herbert, J. M.; Krylov, A. I.; Gill, P. M. W.; Head-Gordon, M. Advances in Molecular Quantum Chemistry Contained in the Q-Chem 4 Program Package. *Mol. Phys.* **2015**, *113* (2), 184–215. https://doi.org/10.1080/00268976.2014.952696.

(54) Rogers, J. P.; Anstöter, C. S.; Bull, J. N.; Curchod, B. F. E.; Verlet, J. R. R. Photoelectron Spectroscopy of the Hexafluorobenzene Cluster Anions: (C6F6)N− (n = 1 – 5) and I−(C6F6). *J. Phys. Chem. A* **2019**. https://doi.org/10.1021/acs.jpca.8b11627.

(55) Martin, J. M. L. Heat of Atomization of Sulfur Trioxide, SO3: A Benchmark for Computational Thermochemistry. *Chem. Phys. Lett.* **1999**, *310* (3), 271–276. https://doi.org/10.1016/S0009-2614(99)00749-6.

(56) Martin, JanM. L. A Fully Ab Initio Quartic Force Field of Spectroscopic Quality for SO3. *Spectrochim. Acta. A. Mol. Biomol. Spectrosc.* **1999**, *55* (3), 709–718. https://doi.org/10.1016/S1386-1425(98)00271-6.

(57) Nimlos, M. R.; Ellison, G. B. Photoelectron Spectroscopy of Silicon Trihydride and Trideuteride Anions. *J. Am. Chem. Soc.* **1986**, *108* (21), 6522–6529. https://doi.org/10.1021/ja00281a013.

(58) Kaldor, A.; Maki, A. G.; Dorney, A. J.; Mills, I. M. The Assignment of N2 and N4 of SO3. *J. Mol. Spectrosc.* **1973**, *45* (2), 247–252. https://doi.org/10.1016/0022-2852(73)90155-0.

(59) Yamada, C.; Hirota, E.; Kawaguchi, K. Diode Laser Study of the N2 Band of the Methyl Radical. *J. Chem. Phys.* **1981**, *75* (11), 5256–5264. https://doi.org/10.1063/1.441991.

(60) Wigner, E. P. On the Behavior of Cross Sections Near Thresholds. *Phys. Rev.* **1948**, *73* (9), 1002–1009. https://doi.org/10.1103/PhysRev.73.1002.

(61) Mabbs, R.; Mbaiwa, F.; Wei, J.; Van Duzor, M.; Gibson, S. T.; Cavanagh, S. J.; Lewis, B. R. Observation of Vibration-Dependent Electron Anisotropy in ${\mathrm{O}}_{2}^{\ensuremath{-}}$ Photodetachment. *Phys. Rev. A* **2010**, *82* (1), 011401. https://doi.org/10.1103/PhysRevA.82.011401.

(62) Bull, J. N.; Anstöter, C. S.; Verlet, J. R. R. Fingerprinting the Excited-State Dynamics in Methyl Ester and Methyl Ether Anions of Deprotonated Para-Coumaric Acid. *J. Phys. Chem. A* **2020**, *124* (11), 2140–2151. https://doi.org/10.1021/acs.jpca.9b11993.

(63) Amrein, A.; Simpson, R.; Hackett, P. Multiphoton Excitation, Ionization, and Dissociation Decay Dynamics of Small Clusters of Niobium, Tantalum, and Tungsten: Time-Resolved Thermionic Emission. *J. Chem. Phys.* **1991**, *95* (3), 1781–1800. https://doi.org/10.1063/1.461026.

(64) Amrein, A.; Simpson, R.; Hackett, P. Delayed Ionization Following Photoexcitation of Small Clusters of Refractory Elements: Nanofilaments. *J. Chem. Phys.* **1991**, *94* (6), 4663–4664. https://doi.org/10.1063/1.460595.

(65) Campbell, E. E. B.; Ulmer, G.; Hertel, I. V. Delayed Ionization of C\textlesssub\textgreater60\textless/Sub\textgreater and

C\textlesssub\textgreater70\textless/Sub\textgreater. *Phys. Rev. Lett.* **1991**, *67* (15), 1986–1988. https://doi.org/10.1103/PhysRevLett.67.1986.

(66) Concina, B.; Lépine, F.; Bordas, C. Thermionic Emission as a Probe of Low-Energy Electron Attachment to Fullerenes. *Phys. Rev. A* **2014**, *90* (3), 033415. https://doi.org/10.1103/PhysRevA.90.033415.

(67) Climen, B.; Pagliarulo, F.; Ollagnier, A.; Baguenard, B.; Concina, B.; Lebeault, M. A.; Lépine, F.; Bordas, C. Threshold Laws in Delayed Emission: An Experimental Approach. *Eur. Phys. J. D* **2007**, *43* (1), 85–89. https://doi.org/10.1140/epjd/e2007-00116-7.

(68) Anstöter, C. S.; Bull, J. N.; Verlet, J. R. R. Ultrafast Dynamics of Temporary Anions Probed through the Prism of Photodetachment. *Int. Rev. Phys. Chem.* **2016**, *35*, 509–538. https://doi.org/10.1080/0144235X.2016.1203522.

(69) Bull, J. N.; West, C. W.; Verlet, J. R. R. On the Formation of Anions: Frequency-, Angle-, and Time-Resolved Photoelectron Imaging of the Menadione Radical Anion. *Chem Sci* **2015**, *6* (2), 1578–1589. https://doi.org/10.1039/C4SC03491K.

(70) Adams, C. L.; Hansen, K.; Weber, J. M. Vibrational Autodetachment from Anionic Nitroalkane Chains: From Molecular Signatures to Thermionic Emission. *J. Phys. Chem. A* **2019**, *123* (40), 8562–8570. https://doi.org/10.1021/acs.jpca.9b07780.

(71) Horke, D. A.; Li, Q.; Blancafort, L.; Verlet, J. R. R. Ultrafast Above-Threshold Dynamics of the Radical Anion of a Prototypical Quinone Electron-Acceptor. *Nat. Chem.* **2013**, *5* (8), 711–717. https://doi.org/10.1038/nchem.1705.

(72) West, C. W.; Bull, J. N.; Antonkov, E.; Verlet, J. R. R. Anion Resonances of Para-Benzoquinone Probed by Frequency-Resolved Photoelectron Imaging. *J. Phys. Chem. A* **2014**, *118* (48), 11346–11354. https://doi.org/10.1021/jp509102p.

(73) Mensa-Bonsu, G.; Lietard, A.; Tozer, D. J.; Verlet, J. R. R. Low Energy Electron Impact Resonances of Anthracene Probed by 2D Photoelectron Imaging of Its Radical Anion. *J. Chem. Phys.* **2020**, *152* (17), 174303. https://doi.org/10.1063/5.0007470.